FULL PAPER

Dalton
www.rsc.org/dalton

Mixed-valence phosphato–hydrogenphosphato–iron network compounds $^1_\infty\{[C_4N_2H_{11.6}]_{1.5}[Fe^{II}Fe^{III}(PO_4)(H_{0.8}PO_4)_2]\cdot H_2O\}$ and $^3_\infty[Fe^{II}_5Fe^{III}_2(PO_4)_2(H_{0.5}PO_4)_4]$: structure elucidation with the help of Mössbauer spectroscopy and a caveat on X-ray diffraction

Khalid Abu-Shandi,[a] Heiner Winkler,[b] Michael Gerdan,[b] Franziska Emmerling,[a] Biao Wu[a] and Christoph Janiak *[a]

[a] *Institut für Anorganische und Analytische Chemie, Universität Freiburg,, Albertstr. 21, D-79104 Freiburg, Germany. E-mail: janiak@uni-freiburg.de; Fax: 49 761 2036147; Tel: 49 761 2036127*

[b] *Institut für Physik, Universität zu Lübeck, Ratzeburger Allee 160, D-23538 Lübeck, Germany*

Received 10th February 2003, Accepted 29th May 2003
First published as an Advance Article on the web 18th June 2003

The mixed-valence iron phosphates $^1_\infty\{[C_4N_2H_{11.6}]_{1.5}[Fe^{II}Fe^{III}(PO_4)(H_{0.8}PO_4)_2]\cdot H_2O\}$ (**1**) and $^3_\infty[Fe^{II}_5Fe^{III}_2(PO_4)_2(H_{0.5}PO_4)_4]$ (**2**) have been synthesized by hydrothermal methods. Their crystal structures were determined by single-crystal X-ray diffraction and Mössbauer spectroscopy. Mössbauer spectroscopy suggests the Fe centers in compound **1** to be mostly in a trapped, mixed-valence +2 and +3 oxidation state from which the average protic hydrogen occupation on HPO_4 and piperazinedium is calculated to be 0.8. At 4 K there is an intervalence tunneling process between part of the Fe^{2+} and Fe^{3+} atoms. Compound **1** contains linear strands of corner-sharing $\{FeO_4\}$ and $\{PO_4\}$ tetrahedra. The Fe atoms are bridged by Fe–O–P–O–Fe and Fe–O–Fe linkages. The strands are held together by hydrogen bonding interactions involving the piperazinedium and the water molecules of crystallization as well as complementary H-bonds between the HPO_4-groups. The iron phosphate **2** is found from Mössbauer spectroscopy to be a trapped mixed-valence system with about 30% Fe^{3+}/70% Fe^{2+} which translates perfectly into $Fe^{II}_5Fe^{III}_2$ from which a total of two protic hydrogens on phosphate has been calculated. The crystal quality permitted the protic hydrogens in **1** and **2** to be found and their positions freely refined. At 4.2 K the Fe^{3+} is completely and Fe^{2+} partially magnetically ordered in **2**. Compound **2** is a three-dimensional framework constructed from edge- and corner-sharing $\{FeO_6\}$ octahedra and $\{FeO_5\}$ trigonal bipyramids together with the $\{PO_4\}$ tetrahedra. Temperature-variable magnetic measurements confirm the oxidation state assignments for **1** and **2** through a matching experimental and calculated value for μ_{eff} at 300 K.

Introduction

Recent years have seen numerous studies on the construction of (hydrogen)phosphato-metal network compounds.[1–14] Metal phosphates with open-framework structures, most notably aluminium phosphates (AlPOs) are of interest because of their potential applications as catalysts, molecular sieves or ion-exchange materials[2,15–17] similar to zeolites.[18] Many such compounds are prepared using organic amines as structure-directing agents by hydrothermal methods.[4–13,17,19–27] With metal atoms such as zinc, aluminium or gallium, there is no problem in the assignment of the oxidation state and subsequently the structure solution in terms of protons on the organic amine and the phosphate groups. The structure solution from single-crystal X-ray diffraction and the formula may be ambigious with metal atoms which can exist in two readily available oxidation states[7,8] since the hydrogen atoms which are crucial for the assignment of the oxidation state are not easily located. On the other hand, it is such metal types that are of particular interest in the construction of open-framework metal compounds for catalytic applications because of their redox activity.[15–17] We show here how Mössbauer spectroscopy is necessary to arrive at a complete structural description of the mixed-valence compounds $^1_\infty\{[C_4N_2H_{11.6}]_{1.5}[Fe^{II}Fe^{III}(PO_4)(H_{0.8}PO_4)_2]\cdot H_2O\}$ (**1**) and $^3_\infty[Fe^{II}_5Fe^{III}_2(PO_4)_2(H_{0.5}PO_4)_4]$ (**2**). This also includes the correction of a recent structural report on "$^3_\infty[Fe^{II}_7(PO_4)_2(HPO_4)_4]$"[28] which has to be correctly formulated as **2**.

Results and discussion

Compound $^1_\infty\{[C_4N_2H_{11.6}]_{1.5}[Fe^{II}Fe^{III}(PO_4)(H_{0.8}PO_4)_2]\cdot H_2O\}$, 1

Hydrothermal treatment of piperazinedium hydrogenphosphate monohydrate[29] with iron(II) chloride in the presence of triethylamine in tetrahydrofuran at 180 °C yielded dark-blue crystals (turning green upon grinding) which have been analyzed as $^1_\infty\{[C_4N_2H_{11.6}]_{1.5}[Fe^{II}Fe^{III}(PO_4)(H_{0.8}PO_4)_2]\cdot H_2O\}$ (**1**) (eqn. (1)) from single-crystal X-ray diffraction and Mössbauer spectroscopy.

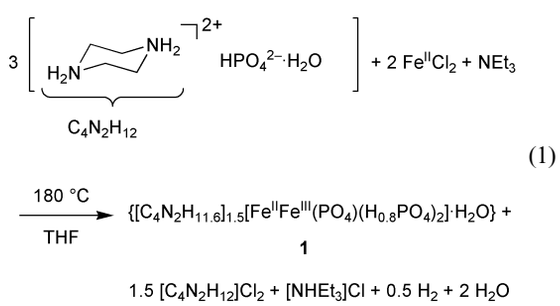

(1)

The hydrogen atoms of the water molecule, the hydrogenphosphato ligands and on the nitrogen atom of the piperazinedium cations in **1** were found in the X-ray data Fourier maps and their atomic positions could be freely refined. Yet, their occupation factors are closely related to the oxidation

DOI: 10.1039/b301610b

Table 1 Mössbauer parameters for compound **1** [a]

Temp./K	Subspectrum	$\delta^{a\text{-}Fe}$ [b]/mm s^{-1}	ΔE_Q [c]/mm s^{-1}	B_{hf} [d]/Tesla	Rel. area (%)
293 (RT)	Narrow doublet	0.41	0.56	–	62.5
	Wide doublet	1.21	2.70	–	37.5
77	Magnetic sextet	0.51	−0.04	28.0	26.0
	Narrow doublet	0.51	0.73	–	35.8
	Wide doublet	1.32	2.91	–	38.2
4.2	Magnetic sextet	0.51	+0.15	48.7	16.3
	Magnetic sextet	0.56	−0.21	52.6	22.8
	Doublet	0.88	1.45	–	26.9
	Magnetic sextet	1.34	−0.88	30.3	34.0

[a] The errors of the hyperfine parameters are about 2% and of the relative areas 5%. [b] Isomer shift. [c] Quadrupole splitting. [d] Magnetic hyperfine field.

state of the iron atoms. A full protic hydrogen occupation of the two hydrogenphosphato groups and the piperazinedium cations translates into an iron oxidation state of Fe(II) within the formula $^1_\infty\{[C_4N_2H_{12}]_{1.5}[Fe^{II}_2(PO_4)(HPO_4)_2]\cdot H_2O\}$. A mixed-valence Fe(II)Fe(III) compound would require an average protic hydrogen content of 0.8 on each HPO_4 and each nitrogen of $C_4N_2H_{10}$, thus $^1_\infty\{[C_4N_2H_{11.6}]_{1.5}[Fe^{II}Fe^{III}(PO_4)(H_{0.8}PO_4)_2]\cdot H_2O\}$ for electroneutrality. Finally, a fully Fe(III) compound would require an average protic hydrogen occupation of 0.6 to give the formula $^1_\infty\{[C_4N_2H_{11.2}]_{1.5}[Fe^{III}_2(PO_4)(H_{0.6}PO_4)_2]\cdot H_2O\}$. These small differences in hydrogen occupation when going from a total of 22 over 21 to 20 hydrogen atoms per formula unit did not reflect in significant changes in the *R*-value during structure refinement. Hence, single-crystal X-ray structure refinement could not lead to an unambiguous formula assignment. Instead of the average fractional occupation factors, full hydrogen occupation on HPO_4^{2-} at the expense of the piperazine groups could, of course, have been assumed. Thus, an alternative formula for the Fe(II)Fe(III) case would have been $^1_\infty\{[C_4N_2H_{10.33}]_{1.5}[Fe^{II}Fe^{III}(PO_4)(HPO_4)_2]\cdot H_2O\}$ or $^1_\infty\{[C_4N_2H_{11}][C_4N_2H_{12}]_{0.5}[Fe^{II}Fe^{III}(PO_4)(HPO_4)_2]\cdot H_2O\}$ if one wants to further differentiate between the two piperazine moieties.

Therefore, it was of primary importance to determine the oxidation state of the iron atoms in **1**. ^{57}Fe Mössbauer spectroscopy can help to determine whether iron atoms are Fe(II), Fe(III)[30] or mixed-valence.[31–34] The room-temperature Mössbauer spectrum of **1** (Fig. 1(a)) can be fitted by two doublets, a narrow one which can be assigned to high-spin Fe(III) and a wide one assigned to high-spin Fe(II) for both of which the observed isomer shift and quadrupole splitting (Table 1) are typical.[35] Subspectra with isomer shifts $\delta^{a\text{-}Fe}$ below 0.7 mm s^{-1} are assigned to Fe^{3+}. The Mössbauer spectrum of **1** recorded at 77 K (Fig. 1(b)) can be fitted by two doublets with about the same parameters as seen in the room temperature spectrum plus a magnetic sextet which originated from part of the Fe(III) doublet. At 4.2 K (Fig. 1(c)) both the Fe^{2+} and Fe^{3+} are magnetically ordered as evident by the appearance of the magnetic sextets and the absence of their wide and narrow doublets, respectively, seen at higher temperature. The hyperfine splitting parameters and the magnetic ordering observed at low temperature in compound **1** are consistent with both Fe(II) ($S = 2$) and Fe(III) ($S = 5/2$) in tetrahedral environment.[35–38] However a new doublet has appeared at 4.2 K with a different isomer shift and quadrupole splitting than seen before for the doublets at higher temperatures. The new doublet comprises intensity from both the Fe^{2+} and Fe^{3+} signal. This new doublet is assigned to an intervalence transition between Fe(II) and Fe(III), that is to a detrapping of the valence states.[32] The fact that the electron exchange is only seen at low temperature but not anymore at high temperature is explained by a tunneling process or a coherent superposition of two states $Fe_A^{2+}Fe_B^{3+}$ and $Fe_A^{3+}Fe_B^{2+}$ instead of a charge transfer process. At higher temperature, thermal vibrations of the Fe atoms destroy the coherence and lead to a valence localization or trapping.[39] The

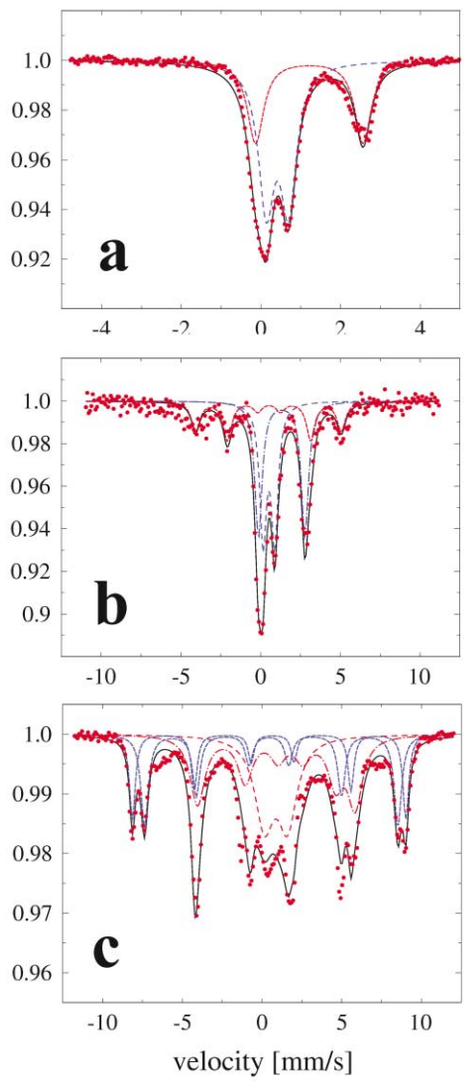

Fig. 1 Mössbauer spectra of **1** at (a) room temperature, (b) $T = 77$ K and (c) 4.2 K. A sum of Lorentzians (solid line, parameters in Table 1) is used to fit the experimental data (dots).

intensity ratio $I_{Fe^{2+}}/I_{Fe^{3+}}$ is less than 1 which in part may be explained with an expected somewhat higher recoil-free fraction for the Fe^{3+} sites. It should also be noted that the line widths for the transitions at RT in Fig. 1(a) are somewhat larger (0.5 mm s^{-1}) than usual (0.25 mm s^{-1}). Such broadening is consistent with Fe^{2+}/Fe^{3+} disorder.[33]

While Mössbauer spectroscopy may suggest a higher Fe(III) content, for simplicity we take the two Fe centers as $Fe^{II}Fe^{III}$ or in the nominal +2.5 oxidation state. Therefore, the formula for **1** would have to be $^1_\infty\{[C_4N_2H_{10+2y}]_{1.5}[Fe^{II}Fe^{III}(PO_4)(H_xPO_4)_2]\cdot$

H_2O} (where $2x + 3y = 4$) or on average $x = y = 0.8$ with $^1{}_\infty$\{$[C_4N_2H_{11.6}]_{1.5}[Fe^{II}Fe^{III}(PO_4)(H_{0.8}PO_4)_2]\cdot H_2O$\}. Hence, the protic hydrogen atom positions on hydrogenphosphate and piperazinedium are not fully occupied. Furthermore, X-ray crystallography as an averaging method cannot unequivocally decide on the protic hydrogen occupation factors in **1** even though the data set was very good (see *R*-values in Table 8). An argument for deviation from an average protic hydrogen occupation between phosphate and piperazine might invoke the difference in acidity constants (pK_a-values) for $[C_4N_2H_{12}]^{2+}$ and HPO_4^{2-} and the species distribution as a function of pH calculated therefrom (see Fig. 2).[40] Such an argument would, however be based on the aqueous solution behavior. The solid state can easily stabilize $[C_4N_2H_{12}]^{2+}/HPO_4^{2-}$ acid–base ratios different from the solution content. Examples have been provided by the structures of $[M(H_2O)_6]^{2+}[C_4N_2H_{12}]^{2+}(HPO_4^{2-})_2$ (M = Co(II), Ni(II)) which could be grown regardless of the solution pH values between 3.5 and 6.2.[29] The structures stabilize the coexistence of $[C_4N_2H_{12}]^{2+}$ and HPO_4^{2-} in a ratio which could not be found in aqueous solution (see Fig. 2). Thus, we decided on an average hydrogen occupation of $H_{0.8}$ over both hydrogenphosphate groups and the piperazinedium cations for **1**.

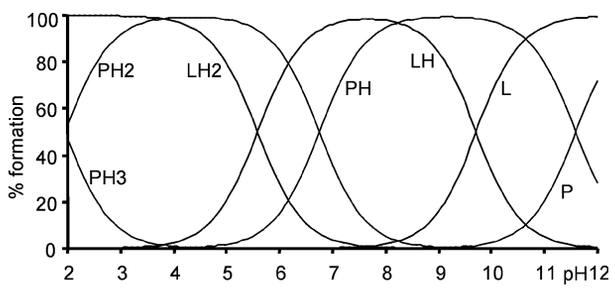

Fig. 2 Species distribution for piperazine/phosphate in the range pH 2–12. pK values: $pK_{PH_3} = 1.92$; $pK_{PH_2} = 6.75$; $pK_{PH} = 11.59$; $pK_{LH_2} = 5.59$; $pK_{LH} = 9.71$; P = PO_4, L = piperazine.

The crystal structure of piperazinedium [bis(μ-hydrogenphosphato)(μ$_4$-phosphato)diferrate(II,III)] hydrate (**1**) consists of columns or strands of {FeO_4} and {PO_4} or {HPO_4} corner-sharing tetrahedra (Fig. 3). The bridging oxygen atoms are provided by the phosphate or hydrogenphosphate groups. Within the column there exist two crystallographically different types of iron atoms and three different phosphate groups. Two phosphate groups are hydrogenphosphate (around P1 and P3); together with the Fe atoms they construct the outer phosphate linkages of the strand. Each HPO_4 group bridges between two Fe atoms with two of its oxygen atoms as Fe–O–P–O–Fe. The remaining phosphate moiety, PO_4^{3-} constructs the central linkers of the strand. The PO_4^{3-} group bridges between four iron

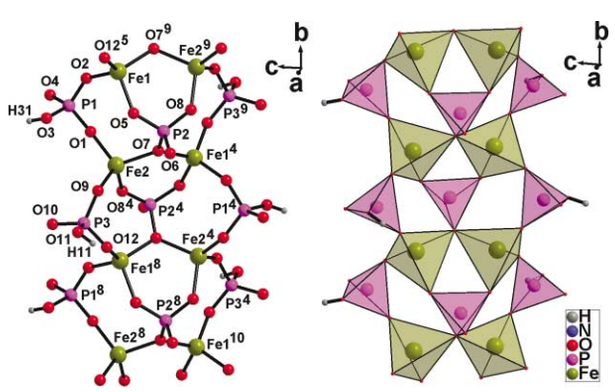

Fig. 3 Section of a single column or strand of $\{Fe_2(PO_4)(H_{0.8}PO_4)_2\}_n$ in **1**. Ball and stick drawing to the left, polyhedral presentation with the central atoms shown in the center of the tetrahedra on the right; the columns run along the *b*-axis. Symmetry transformations: $^4 = -x - 1$, $y - 1/2$, $-z - 1/2$; $^5 = x$, $y + 1$, z; $^8 = x$, $y - 1$, z; $^9 = -x - 1$, $y + 1/2$, $-z - 1/2$; $^5 = -x - 1$, $y - 3/2$, $-z - 1/2$.

Table 2 Selected bonds lengths (Å) and angles (°) in compound **1** [a]

Fe1–O2	1.9227(14)	Fe2–O9	1.9277(14)
Fe1–O12#5	1.9396(14)	Fe2–O1	1.9488(14)
Fe1–O5	1.9936(13)	Fe2–O8#4	1.9729(14)
Fe1–O7#9	1.9967(13)	Fe2–O7	1.9993(13)
O2–Fe1–O12#5	116.81(6)	O9–Fe2–O1	116.44(7)
O2–Fe1–O5	106.06(6)	O9–Fe2–O8#4	108.65(6)
O12#5–Fe1–O5	98.10(6)	O1–Fe2–O8#4	101.74(6)
O2–Fe1–O7#9	110.56(6)	O9–Fe2–O7	110.56(6)
O12#5–Fe1–O7#9	116.70(6)	O1–Fe2–O7	112.40(6)
O5–Fe1–O7#9	106.70(5)	O8#4–Fe2–O7	106.12(5)

[a] Symmetry transformations used to generate equivalent atoms: #4 = $-x - 1$, $y - 1/2$, $-z - 1/2$; #5 = x, $y + 1$, z; #8 = x, $y - 1$, z; #9 = $-x - 1$, $y + 1/2$, $-z - 1/2$; #10 = $-x - 1$, $y - 3/2$, $-z - 1/2$.

atoms using three of its oxygen atoms. Two of these Fe atoms are joined by a single oxygen atom Fe–O–Fe bridge whereas the other bridges consist of the usual Fe–O–P–O–Fe type. In addition to its bridging mode the last phosphate group is chemically different from the other two HPO_4 groups by not carrying a hydrogen atom. Bond distances and angles between non-hydrogen atoms are listed in Table 2. The Fe–O distances are in the expected range.[41–43]

Neighboring strands are connected through hydrogen bonding interactions. One type of the hydrogen bonding is provided by complementary H-bonds between the HPO_4 groups of P1 in the *bc*-plane (Fig. 4(a)). The cavities thus formed contain the piperazinedium counter cations and water molecules of

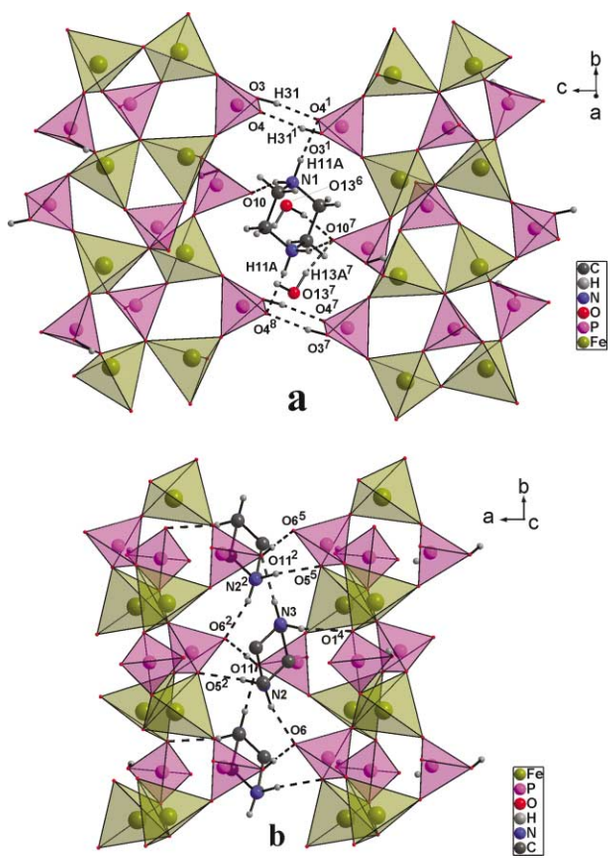

Fig. 4 Connection of neighboring strands of $\{Fe_2(PO_4)(H_{0.8}PO_4)_2\}_n$ in **1**; (a) within the *bc*-plane, showing the complementary hydrogen bonding between the HPO_4 groups from P1, the piperazinedium cations $[C_4N_2H_{11.6}]^{2+}$ and the water molecules of crystallization; (b) within the *ab*-plane, hydrogens on carbon omitted for clarity. N and C of $[C_4N_2H_{11.6}]^{2+}$ can be superimposed. Distances and angles of the hydrogen bonding interaction are given in Table 3. The protic hydrogen atoms on HPO_4 and on piperazine, $C_4N_2H_{10}$ are not fully occupied; see text. Symmetry transformations: $^1 = -x + 1$, $-y + 1$, $-z$; $^2 = -x$, $y - 1/2$, $-z - 1/2$; $^4 = -x - 1$, $y - 1/2$, $-z - 1/2$; $^5 = x$, $y + 1$, z; $^6 = x + 1$, y, z; $^7 = -x + 1$, $-y$, $-z$; $^8 = x$, $y - 1$, z.

Table 3 Hydrogen bonding interactions (Å, °) in **1**[a]

D–H ··· A	D–H	H ··· A	D ··· A	D–H ··· A
O3–H31 ··· O4#1	0.75(4)	1.87(4)	2.608(2)	173(4)
O11–H11 ··· O6#2	0.88(3)	1.66(3)	2.532(2)	174(3)
O13–H13A ··· O10	1.05(3)	1.86(3)	2.900(3)	168(3)
O13–H13B ··· O10#3	1.04(3)	1.91(3)	2.942(3)	170(3)
N1–H11A ··· O4#1	0.94(3)	1.88(3)	2.812(2)	168(2)
N1–H12B ··· O10	0.94(3)	1.75(3)	2.664(4)	165(2)
N2–H21A ··· O6	0.94(3)	1.84(3)	2.754(4)	166(2)
N2–H22B ··· O5#2	0.95(3)	1.88(3)	2.817(2)	169(2)
N3–H31A ··· O1#4	0.92(3)	2.08(3)	2.909(3)	148(3)
N3–H31A ··· O4#4	0.92(3)	2.31(3)	3.079(2)	141(2)
N3–H31B ··· O11#2	0.90(3)	1.98(3)	2.837(2)	157(3)

[a] The hydrogen atom position are not fully occupied; see text; D = donor, A = acceptor. Symmetry transformatios: #1 = $-x-1, -y+1, -z$; #2 = $-x, y-1/2, -z-1/2$; #3 = $-x, -y, -z$; #4 = $-x-1, y-1/2, -z-1/2$.

crystallization. These cations and water provide for additional hydrogen bonding to the hydrogenphosphate groups and thereby also connect the adjacent columns in the *ab*-plane (see Fig. 4(b)).

Similar one-dimensional metal phosphate chains containing corner-sharing tetrahedra were reported for $^1_\infty\{[C_5N_2H_{12}][Co(HPO_4)_2]\}$,[44] $^1_\infty\{[H_3N(CH_2)_2NH_3][Al(PO_4)(HPO_4)]\}$[45] and $^1_\infty\{[H_3N(CH_2)_4NH_3][Ga(PO_4)(HPO_4]\}$.[46] To the best of our knowledge, no example of chains based on corner-sharing tetrahedra of iron-phosphate has been reported.

Bond valence sum calculations done on the iron atoms of **1** gave a value of 2.31 for Fe1 and 2.32 for Fe2 (both with the parameter R_0 for Fe^{3+}).[47,48] This deviates somewhat from an expected value of 2.5 for a mixed-valence $Fe^{II}Fe^{III}$ system. There may be a larger Fe(III) content in **1** as hinted by the Mössbauer data. Furthermore, we ascribe part of this deviation to the tetrahedral coordination of the iron atoms in **1**, as the bond valence sum calculations appear to be parametrized more on structures of penta- and hexacoordinated iron atoms.

Temperature-variable magnetic measurements on **1** support the oxidation state assignment of $Fe^{II}Fe^{III}$. The experimental magnetic moment $\mu_{eff} = 8.2\ \mu_B$ at 300 K derived from $(8\chi T)^{1/2}$ is in good agreement with the calculated spin-only value for a magnetically uncoupled system of $\mu_{eff} = 7.68\ \mu_B$ [$\mu_{eff} = (\Sigma 4S_i(S_i + 1))^{1/2}\mu_B$ with $S_1 = 2$ for Fe(II) and $S_2 = 5/2$ for Fe(III)]. The larger experimental value is traced to contributions from spin–orbit coupling for the Fe(II) atom. The decrease of μ_{eff} with temperature (Fig. 5) indicates a weak antiferromagnetic interaction. The data could be fitted with $J = 17.2\ cm^{-1}$ ($\boldsymbol{H}_{exchange} = J\boldsymbol{S}_1\cdot\boldsymbol{S}_2$) and $g_{eff} = 2.37$ for Fe(II) with $g_{eff} = 2$ kept constant for Fe(III).

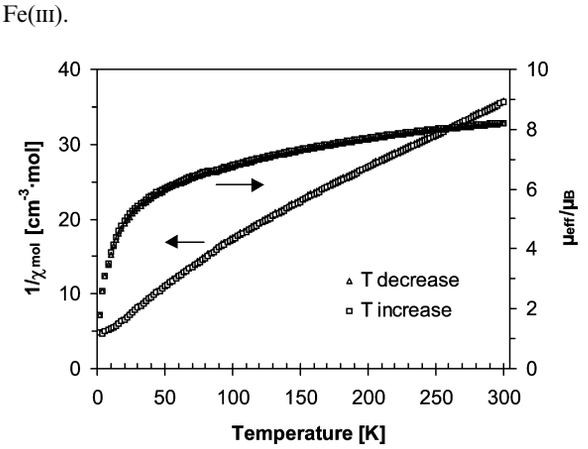

Fig. 5 Magnetic data for compound **1**.

Compound $^3_\infty[Fe^{II}_5Fe^{III}_2(PO_4)_2(H_{0.5}PO_4)_4]$, 2

The iron phosphate **2** was obtained from the hydrothermal combination of *N*-methylpiperazinedium phosphate with iron(II) chloride in water. The analysis of the black–green crystals relied on the use of ^{57}Fe Mössbauer spectroscopy for the determination of the iron oxidation state, and hence the protic hydrogen content on the phosphato ligands. The Mössbauer spectrum for compound **2** at room temperature (Fig. 6(a)) can be fitted with four subspectra as the sum of one narrow doublet, two doublets and one magnetic sextet. At liquid helium temperature of 4.2 K the Mössbauer spectrum (Fig. 6(c)) can be fitted with five subspectra as the sum of two doublets and three magnetic sextets. At the intermediate temperature of 77 K (Fig. 6(b)), also five subspectra are required to fit the Mössbauer spectrum: three magnetic sextets, one narrow doublet and one wide doublet. Subspectra with isomer shifts, $\delta^{\alpha\text{-Fe}}$ below 0.6 mm s^{-1} are again assigned to Fe^{3+}. This is consistent with the large magnetic splitting around 50 Tesla. Thus, Fe^{3+} is completely magnetically ordered at 4.2 K. The relative area content of these Fe^{3+} species is around 30%. The large isomer shifts of the remaining subspectra with $\delta^{\alpha\text{-Fe}} > 1$ mm s^{-1} are indicative of Fe^{2+} ($S = 2$). Their relative area content corresponds to about 70%. These area ratios closely match a molar Fe(II)/Fe(III) ratio of 5 : 2 (71.4 : 28.6%) as $Fe^{II}_5Fe^{III}_2$ in **2**. Also Fe^{2+} is increasingly magnetically ordered with lower temperature. Magnetic ordering has also been reported in other iron phosphates, *e.g.* $^2_\infty\{[Fe^{III}_2(H_2O)_2(O_3PCH_2PO_3H)_2]\cdot 2H_2O_2\}$ (antiferromagnetic),[49] $^1_\infty\{[H_3N(CH_2)_4NH_3][Fe^{III}_2\{CH_3C(OH)(PO_3)(PO_3H)\}_2]\cdot 2H_2O\}$ (ferromagnetic),[50] $^2_\infty\{[H_3NCH_2CH_2NH_3]_{0.5}[Fe^{III}(OH)(PO_4)]\}$ (weak antiferromagnetic)[51] and $^3_\infty\{[H_3NCH_2CH_2NH_3]_2[Fe_4O(PO_4)_4]\cdot H_2O\}$ (trapped mixed valence, trigonal-bipyramidal Fe, anti- or canted antiferromagnetic).[33,52] In addition to these aforementioned examples, Mössbauer data are also available for other iron phosphates with octahedrally coordinated metal centers, *e.g.* $^1_\infty\{[C_4N_2H_{12}]_{1.5}[Fe^{III}_2(OH)(PO_4)(HPO_4)_2(H_2PO_4)]\cdot 0.5H_2O\}$[42] and $^3_\infty\{[(C_4N_3H_{16})(C_4N_3H_{15})][Fe^{III}_5F_4(H_2PO_4)(HPO_4)_3(PO_4)_3]\cdot H_2O\}$ (spin crossover),[53] $^3_\infty\{[C_4N_2H_{12}][Fe_4(OH)_2(HPO_4)_5]\}$ (mixed valence) and $^2_\infty\{[C_4H_{11}N_2]_{0.5}[Fe_3(HPO_4)_2(PO_4)(H_2O)]$ (mixed valence, also trigonal-bipyramidal Fe).[43]

An iron subset of $Fe^{II}_5Fe^{III}_2$ in **2** corresponds to a cationic charge of +16. This charge has to be matched by the six phosphate groups. Electroneutrality then requires a total of two protic hydrogens on the phosphato ligands to arrive at a total anionic charge of −16. In the absence of other OH containing groups in **2** we could use the intensity of the OH-stretching frequency at about 3330 cm^{-1} to quantify the HPO_4 content by infrared spectroscopy. By employing the standard addition method we have followed the intensity of the OH band upon additions of exact aliquots of $NaHPO_4$ (1.0(1) mg, 7.0(7) μmol each) to a sample of **2** (1.0(1) mg, 1.0(1) μmol). Taking into account the blind value for KBr (50 mg) we estimate 2.5(10) μmol HPO_4/μmol of **2**.

Compound **2** is isostructural to an iron phosphate reported by Zhou *et al*. with a formula of $^3_\infty[Fe^{II}_7(PO_4)_2(HPO_4)_4]$ (**2′**) and iron fully in the +2 oxidation state because of an assumed full hydrogen occupancy on the four hydrogenphosphate groups.[28]

Table 4 Mössbauer parameters for compound **2**[a]

Temp./K	Subspectrum	$\delta^{\alpha\text{-Fe}}$[b]/mm s^{-1}	ΔE_Q[c]/mm s^{-1}	B_{hf}[d]/Tesla	Rel. area (%)
293 (RT)	Narrow doublet	0.56	0.23	–	27.5
	Magnetic sextet	1.11	0.00	11.1	9.5
	Doublet	1.15	1.82	–	25.8
	Doublet	1.22	2.62	–	37.2
77	Magnetic sextet	0.42	−1.13	44.9	8.6
	Magnetic sextet	0.55	0.31	48.7	19.9
	Narrow doublet	0.56	0.34	–	2.4
	Doublet	1.38	2.60	–	60.0
	Magnetic sextet	1.35	0.00	11.0	9.1
4.2	Magnetic sextet	0.35	−1.03	48.0	5.5
	Magnetic sextet	0.57	0.25	54.8	23.9
	Doublet	1.31	1.22	–	17.8
	Magnetic sextet	1.37	0.14	15.1	25.8
	Doublet	1.43	3.21	–	27.0

[a] The errors of the hyperfine parameters are about 2% and of the relative areas 5%. [b] Isomer shift. [c] Quadrupole splitting. [d] Magnetic hyperfine field.

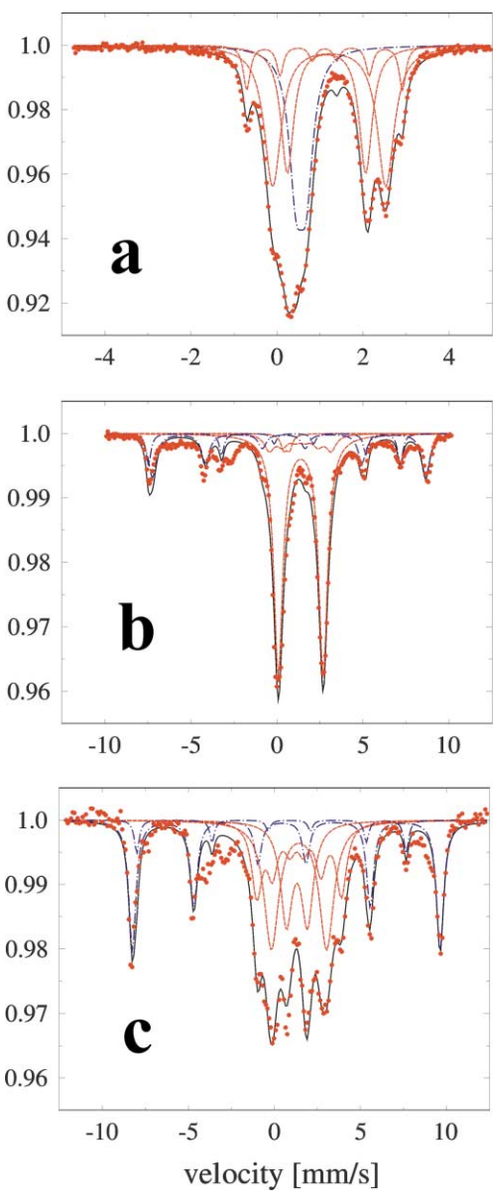

Fig. 6 Mössbauer spectra for compound **2** at (a) room temperature (b) T = 77 K and (c) T = 4.2 K. A sum of Lorentzians (solid line) is used to fit the experimental data (dots); see Table 4 for individual parameters.

The latter compound was made by a different procedure, reacting $FeCl_2$, H_3PO_4 and imidazole in water–ethylene glycol under hydrothermal conditions. Crystals of both synthetic procedures

Table 5 Comparison between cell parameters of compound **2** and **2′**

	Compound **2**	Compound **2′**[28]
Assignment	$Fe^{II}_5Fe^{III}_2$, $H_{0.5}PO_4$	Fe^{II}_7, HPO_4
Symmetry cell	Triclinic	Triclinic
Space group	$P\bar{1}$	$P\bar{1}$
T/K	293	293
a/Å	6.562(3)	6.528(3)
b/Å	7.980(4)	7.956(4)
c/Å	9.536(4)	9.501(4)
α/°	103.874(6)	104.03(4)
β/°	109.286(6)	109.17(2)
γ/°	101.577(6)	101.66(3)
V/Å^3	435.7(3)	430.3 (3)

(ours and Zhou's) agree in their black–green color. Furthermore, Table 5 shows the agreement in the cell parameters and Fig. 7 between the X-ray powder diffractograms for the two structure determinations. Therefore, we suggest that compound **2** and **2′** is the same material and that the hydrogen occupancy has not been correctly assigned in compound **2′**. Furthermore, compound **2** is similar in formula to two reported iron phosphate compounds, namely $Fe_7(PO_4)_5(HPO_4)$[54] and $Fe_7(PO_4)_6$.[55] The simulated X-ray powder diffractograms for the latter two compounds (not shown here), however, exhibit different patterns than for compound **2**.

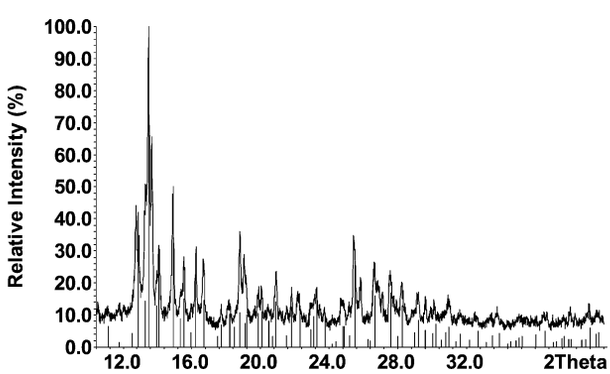

Fig. 7 Measured X-ray powder diffractogram for the crystals of **2** (upper diffractogram) and the simulated diffractogram for the reported compound **2′** (lower diffractogram as vertical bars). The simulated diffractogram from the X-ray structure of **2** (not included) also matches the experimental diffractogram.[56]

The crystal structure of compound **2** (**2′**) consists of {FeO_6} (Fe1, Fe3 and Fe4) and {FeO_5} (Fe2) polyhedra and {PO_4} tetrahedra sharing edges (Fe4–Fe4) or corners to form a three-dimensional framework (Fig. 8). Compound **2** has three types of geometry around the four crystallographically different Fe

Table 6

D–H ··· A	D-H	H ··· A	D ··· A	D–H ··· A
O11–H11 ··· O34#2	0.96(12)	1.54(13)	2.486(4)	166(12)
O22–H22 ··· O23#16	0.84(2)	1.91(2)	2.705(4)	158(2)

D = Donor, A = acceptor. Symmetry transformations: #2 = $x-1, y-1, z$; #16 = $-x, -y-1, -z+1$; [17] = $-x-1, -y-1, -z+1$.

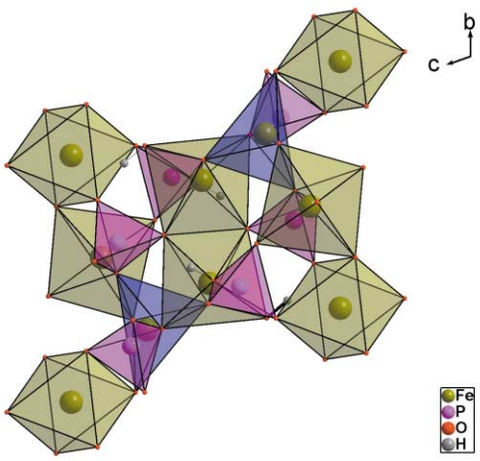

Fig. 8 Polyhedral drawing for a section of compound **2**, showing the edge-sharing between the adjacent Fe4 octahedra. The five-coordinated polyhedra around Fe2 are depicted in blue.

centers. Atom Fe4 is located at a crystallographic inversion center and has a regular octahedral coordination environment, while atoms Fe1 and Fe3 display distorted octahedral coordination environments (Fig. 9(a)). Atom Fe2 is surrounded by five O atoms from three different phosphate groups in a geometry intermediate between trigonal-bipyramidal and square-pyramidal ($\tau = 0.53$)[57] (Fig. 9(b)). The tetrahedral phosphate groups provide for the iron-coordinating and bridging oxygen atoms. All of the phosphate oxygen atoms bridge between iron atoms except for O11, O22, O23 and O34. The first two carry (in part) a hydrogen atom as an O–H group, the last two are (in part) the hydrogen bond acceptors (Fig. 10). In total the phosphate groups of P1 and P3 each connect seven iron atoms, group P2 connects six iron atoms. The differences in the oxygen atom characteristics (bridging *versus* non-bridging) are in agreement with the hydrogen-bonding scheme (Fig. 10 and below). Bond distances and angles between non-hydrogen atoms are listed in Table 7. The Fe–O distances are in the expected range.[41–43]

The oxygen atoms of the OH groups do not bridge between iron atoms and form hydrogen bonds to equally non-bridging oxygen atoms (Fig. 10). The hydrogen bond from (P1–)O11–H11 is formed to an oxygen atom of a *cis*-positioned PO_4 group (around P3) which is bound to the same iron atom (Fe4). This gives rise to a six-membered ring. The hydrogen bond from (P2–)O22–H22 is a complementary one, formed to an oxygen atom on a symmetry related P2 ligand.

Bond valence sum calculations done on the iron atoms of **2** gave values of 2.11 (R_0 for Fe^{2+}) or 2.25 (R_0 for Fe^{3+}) for Fe1, 1.85 or 1.98 for Fe2, 2.04 or 2.19 for Fe3 and 1.78 or 1.91 for Fe4.[47,48] While this may be interpreted in agreement with an all Fe(II) compound[28] it can also be seen in agreement with an $Fe^{II}_5Fe^{III}_2$ system. If out of the four crystallographically different iron positions Fe2 (occupation factor 1) and Fe4 (occupation 0.5) are taken as Fe(II)-only, then the two +3 charges are distributed over the four iron atoms of Fe1 and Fe3 (occupation 1, each), averaging to a charge of +2.5 for each iron atom. If only Fe4 is taken as Fe(II)-only (because the calculation on the five-coordinate Fe2 may be seen as less reliable) then the two +3 charges are distributed over six iron atoms averaging to +2.33 for each iron atom. This latter value is not far from the calcu-

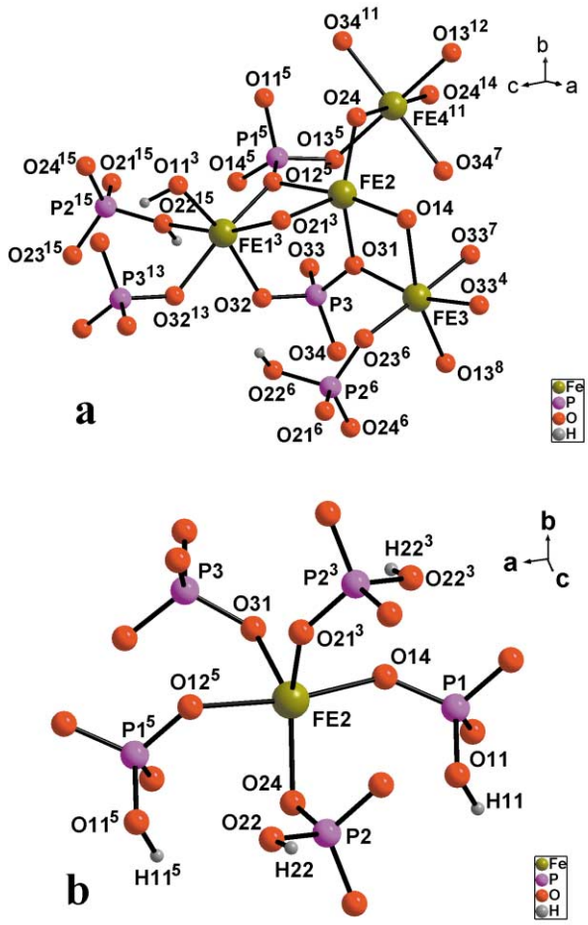

Fig. 9 (a) Section of the structure of **2** showing the geometry around Fe atom centers. (b) The five-coordinated geometry around Fe2 atom (τ = 0.53).[57] The hydrogen atoms are not fully occupied, see text. Symmetry transformations: [3] = $-x, -y, -z+1$; [4] = $x-1, y, z$; [5] = $x+1, y, z$; [6] = $x, y+1, z$; [7] = $-x+1, -y+1, -z+2$; [8] = $-x, -y+1, -z+2$; [11] = $x, y-1, z$; [12] = $-x, -y, -z+2$; [13] = $-x+1, -y+1, -z+1$; [14] = $-x+1, -y, -z+2$; [15] = $-x+1, -y, -z+1$.

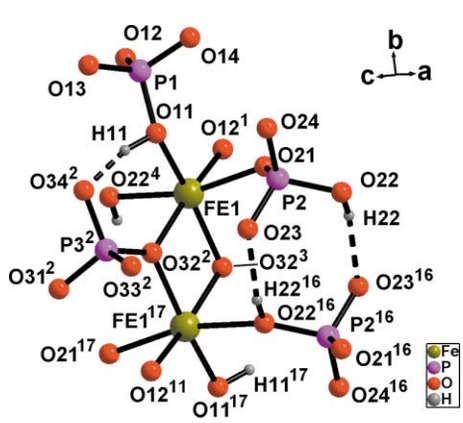

Fig. 10 Section of the structure of compound **2** showing the hydrogen bonding interaction (dashed lines). The hydrogen atoms are not fully occupied, see text. Distances (Å) and angles (°) for the hydrogen bonds are given in Table 6. For symmetry transformations see Tables 6 and 7 and Fig. 9.

Table 7 Selected bond lengths/Å and angles/° in compound **2**[a]

Fe1–O12#1	2.087(2)	Fe3–O23#6	2.062(2)
Fe1–O32#2	2.111(2)	Fe3–O33#7	2.087(2)
Fe1–O32#3	2.113(2)	Fe3–O33#4	2.139(2)
Fe1–O11	2.113(2)	Fe3–O31	2.141(2)
Fe1–O21	2.147(2)	Fe3–O13#8	2.153(2)
Fe1–O22#4	2.164(2)	Fe3–O14	2.238(2)
Fe2–O24	2.036(2)	Fe4–O34,~#9	2.134(2)
Fe2–O31	2.039(2)	Fe4–O13#8+#10	2.169(2)
Fe2–O21#3	2.110(2)	Fe4–O24#6+#7	2.257(2)
Fe2–O14	2.145(2)		
Fe2–O12#5	2.203(2)		
O12#1–Fe1–O32#2	166.20(9)	O23#6–Fe3–O33#7	178.83(9)
O12–1–Fe1–O32#3	90.65(9)	O23#6–Fe3–O33#4	94.27(9)
O32#2–Fe1–O32#3	78.16(10)	O33#7–Fe3–O33#4	85.66(8)
O12#1–Fe1–O11	104.96(9)	O23#6–Fe3–O31	90.06(9)
O32#2–Fe1–O11	87.22(9)	O33#7–Fe3–O31	89.64(8)
O32#3–Fe1–O11	162.98(9)	O33#4–Fe3–O31	161.55(9)
O12#1–Fe1–O21	79.45(8)	O23#6–Fe3–O13#8	96.80(9)
O32#2–Fe1–O21	109.21(8)	O33#7–Fe3–O13#8	84.37(9)
O32#3–Fe1–O21	94.71(9)	O33#4–Fe3–O13#8	91.44(8)
O11–Fe1–O21	81.80(9)	O31–Fe3–O13#8	105.86(9)
O12#1–Fe1–O22#4	91.38(9)	O23#6–Fe3–O14	98.21(9)
O32#2–Fe1–O22#4	82.31(9)	O33#7–Fe3–O14	80.62(9)
O32#3–Fe1–O22#4	97.92(9)	O33#4–Fe3–O14	83.42(8)
O11–Fe1–O22#4	88.60(9)	O31–Fe3–O14	78.21(8)
O21–Fe1–O22#4	164.48(10)	O13#8–Fe3–O14	164.45(8)
O24–Fe2–O31	139.59(9)	O34–Fe4–O34#9	180
O24–Fe2–O21#3	122.35(9)	O34–Fe4–O13#8	89.29(9)
O31–Fe2–O21#3	95.17(9)	O34#9–Fe4–O13#8	90.71(9)
O24–Fe2–O14	104.28(8)	O13#8–Fe4–O13#10	180
O31–Fe2–O14	82.61(9)	O34–Fe4–O24#6	90.29(8)
O21#3–Fe2–O14	97.95(8)	O34#9–Fe4–O24#6	89.71(8)
O24–Fe2–O12#5	84.54(8)	O13#8–Fe4–O24#6	92.56(8)
O31–Fe2–O12#5	90.03(8)	O13#10–Fe4–O24#6	87.44(8)
O21#3–Fe2–O12#5	77.71(8)	O24#6–Fe4–O24#7	180
O14–Fe2–O12#5	171.13(8)		

[a] Symmetry transformations used to generate equivalent atoms: #1 = $-x-1, -y, -z+1$; #2 = $x-1, y-1, z$; #3 = $-x, -y, -z+1$; #4 = $x-1, y, z$; #5 = $x+1, y, z$; #6 = $x, y+1, z$; #7 = $-x+1, -y+1, -z+2$; #8 = $-x, -y+1, -z+2$: #9 = $-x+1, -y+2, -z+2$; #10 = $x+1, y+1, z$; #11 = $x, y-1, z$.

lated charges for Fe1 and Fe3 (with R_0 for Fe^{3+}). Furthermore, we note that the X-ray structure data set of **2** was collected at room temperature, while the bond valence sum calculations appear to be parametrized on low-temperature data sets. The expected, even slight, contraction of the Fe–O bond lengths at lower temperature will increase the calculated charge on the Fe atoms.

Temperature-variable magnetic measurements on **2** support the oxidation state assignment of $Fe^{II}_5Fe^{III}_2$. The experimental magnetic moment of $\mu_{eff} = 13.9\ \mu_B$ at 300 K derived from $(8\chi T)^{1/2}$ is in excellent agreement with the calculated spin-only value of a magnetically uncoupled system of $\mu_{eff} = 13.78\ \mu_B$ [$\mu_{eff} = (\Sigma 4S_i(S_i + 1))^{1/2}\mu_B$ with $S_{1-5} = 2$ for Fe(II) and $S_{6-7} = 5/2$ for Fe(III)]. The temperature dependence of the reciprocal magnetic susceptibility (Fig. 11) indicates an antiferromagnetically ordered structure with a Neel point at $T_N \approx 20$ K. The decrease in $1/\chi$ (increase in χ) below 8 K may be due to paramagnetic impurities, a weak ferromagnetic interaction or non-colinear spin structures because of spin–orbit coupling which also can lead to a weak ferromagnetism.[58] The calculation of the antiferromagnetic exchange interaction is difficult in such a case.

Experimental

IR spectra (KBr pellet) were measured on a Bruker Optik IFS 25. For a quantitative assessment of HPO_4 for compound **2** by the standard addition method 50.0(1) mg of dry KBr and 1.0(1) mg, 1.0(1) μmol of compound **2** were finely ground until a uniform mixture was obtained and pressed into a transparent pellet. After the measurement the pellet is pulverized again and

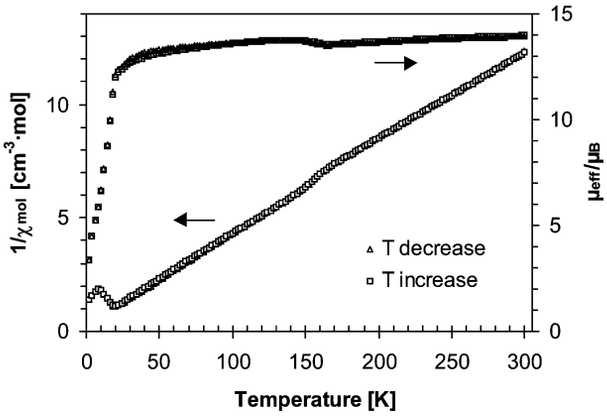

Fig. 11 Magnetic data for compound **2**.

1.0(1) mg, 7.0(7) μmol of Na_2HPO_4 (dried in vacuum, 1×10^{-3} Torr) is added, ground and the pellet pressed again. The last sequence of addition of Na_2HPO_4 was repeated 4 times. The absorbance of the IR band at 3330 cm^{-1} was measured and plotted against the added molar amount of Na_2HPO_4. The blind value for KBr and moisture taken up during the sample preparation was determined the same way without addition of **2**. Extension of the regression lines ($R = 0.99878$ with **2**, 0.99773 blind value) onto the negative abscissa gave 16.3(5) (with **2**) – 13.8(5) (blind value) = 2.5(10) μmol HPO_4/μmol of **2**. Elemental analyses were obtained on a VarioEL from Elementaranalysensysteme GmbH. X-Ray powder diffractometry was done on a Stoe STADI P with Debye–Scherrer geometry, Mo-Kα radiation ($\lambda = 0.7093$ Å) and a Ge(111) monochromator and the samples in glass capillaries on a rotating probe head. $FeCl_2 \cdot 3H_2O$ was obtained from Merck.

^{57}Fe Mössbauer spectroscopy

^{57}Fe Mössbauer spectra were recorded with a conventional spectrometer in constant-acceleration mode with a ^{57}Co[Rh] source. The velocity calibration was performed with an α-Fe foil at room temperature, for which the magnetic hyperfine splitting is known with high accuracy. The measured isomer shifts are referred to this α-Fe standard. The experimental spectra were fitted by a sum of Lorentzian lines by means of a least-squares procedure.

X-Ray crystallography

Data collection. Bruker AXS with CCD area-detector, Mo-Kα radiation ($\lambda = 0.71073$ Å), graphite monochromator, double-pass method ϕ–ω-scan, Data collection and cell refinement with SMART,[59] data reduction with SAINT,[59] experimental absorption correction with SADABS.[60] *Structure analysis and refinement*: The structure was solved by direct methods (SHELXS-97);[61] refinement was done by full-matrix least squares on F^2 using the SHELXL-97 program suite.[61] All non-hydrogen positions were found and refined with anisotropic temperature factors. In **1** the hydrogen atoms of the water molecule, the hydrogenphosphato ligands and on nitrogen of the piperazinedium cation were found and refined with $U_{eq}(H) = 1.2\ U_{eq}(O,N)$. Hydrogen atoms on carbon of piperazinedium were calculated with appropriate riding models (AFIX 23) and $U_{eq}(H) = 1.2\ U_{eq}(C)$. In **2** the hydrogen atom on O11 of the hydrogenphosphato ligand around P1 could be found and refined with $U_{eq}(H) = 10.08$. The hydrogen atom on O22 on P2 could initially also be found but had subsequently to be refined with an appropriate riding model (AFIX 84) and $U_{eq}(H) = 10.08$. Graphics were obtained with DIAMOND.[62] Crystal data and details on the structure refinement are given in Table 8.

CCDC reference numbers 203657 and 203658.

See http://www.rsc.org/suppdata/dt/b3/b301610b/ for crystallographic data in CIF or other electronic format.

Table 8 Crystal data for compounds **1** and **2**

	1	**2**
Formula	$C_6H_{21}Fe_2N_3O_{13}P_3$	$HFe_{3\cdot5}O_{12}P_3$
M	547.87	481.39
Crystal size/mm	0.29 × 0.14 × 0.12	0.51 × 0.11 × 0.11
Crystal description	Plates	Isometric
T/K	213(2)	293(2)
θ Range/°	2.44–28.89	2.40–28.64
h; k; l Range	−11,11;−11,11;−30,31	−8,8;−10,10;−12,12
Crystal system	Monoclinic	Triclinic
Space group	$P2_1/c$	$P\bar{1}$
a/Å	8.370(2)	6.562(3)
b/Å	8.562(2)	7.980(4)
c/Å	23.865(4)	9.536(4)
α/°	90	103.874(6)
β/°	93.950(3)	109.286(6)
γ/°	90	101.577(6)
V/Å^3	1706.2(5)	435.7(3)
Z	4	2
D/g cm^{-3}	2.133	3.669
F(000)	1116	466
μ/mm^{-1}	2.057	6.351
Absorption correction	SADABS	SADABS
Max./min. transmission	0.7904/0.5869	1.000/0.5467
Measured reflections	14884	3935
Unique reflections (R_{int})	4137 (0.0186)	2030 (0.0185)
Obs. reflections [$I > 2\sigma(I)$]	3487	1773
Parameters refined	274	173
Max/min $\Delta\rho$/e Å^{-3} [a]	0.451/−0.577	0.620/−0.729
$R1/wR2$ [$I > 2\sigma(I)$] [b]	0.0240/0.0637	0.0283/0.0699
$R1/wR2$ (all data) [b]	0.0295/0.0659	0.0329/0.0712
Goodness-of-fit on F^2 [c]	1.036	1.027
Weight. scheme w; a/b [d]	0.0405/0.2957	0.0410/0.0000

[a] Largest difference peak and hole. [b] $R1 = [\Sigma(||F_o| - |F_c||)/\Sigma|F_o|]$; $wR2 = [\Sigma[w(F_o^2 - F_c^2)^2]/\Sigma[w(F_o^2)^2]]^{1/2}$. [c] Goodness-of-fit = $[\Sigma[w(F_o^2 - F_c^2)^2]/(n - p)]^{1/2}$. [d] $w = 1/[\sigma^2(F_o^2) + (aP)^2 + bP]$ where $P = (\max(F_o^2 \text{ or } 0) + 2F_c^2)/3$.

Magnetic measurements

Magnetic data were collected at 1 Tesla with a MPMS 5 SQUID magnetometer (Quantum Design, USA) between 300 and 2 K in steps of 2 K. Susceptibility data were collected during one cooling and one heating cycle. The hysteresis was too small to assign any significance to it.

Synthesis

Piperazinedium [bis(μ-hydrogenphosphato)(μ$_4$-phosphato)-diferrate(II,III)] hydrate, $^1{}_\infty\{[C_4N_2H_{11.6}]_{1.5}[Fe^{II}Fe^{III}(PO_4)(H_{0.8}PO_4)_2]\cdot H_2O\}$, (1). Under a positive pressure of argon $FeCl_2\cdot 3H_2O$ (0.353 g, 1.50 mmol) was dispersed in 5 mL of degassed THF in a Schlenk flask to give a yellowish–green, clear solution. To this solution piperazinedium hydrogenphosphate monohydrate[29] (0.60 g, 3.0 mmol) was added with continuous stirring, followed by triethylamine (TEA) (0.65 mL, 4.70 mmol). The TEA was needed to adjust the pH of the resulting solution to around 8. The mixture was stirred at room temperature for 30 min. The solution was transferred to a Teflon-lined stainless-steel autoclave and heated at 180 °C for 40 h followed by slow cooling at a rate of 10 °C min^{-1}. Dark blue crystals were collected by filtration (yield 170 mg, 41%). The blue crystals turned green upon grinding. $C_6H_{21}Fe_2N_3O_{13}P_3$ (547.87): calc.: C 13.15, H 3.86, N 7.67; found: C 13.27, H 4.13, N 7.69%. IR (major peaks only): 3440 (br, νOH), 2976 (νC–H), 1466 (νP=O), 985 (νP–O).

Over a period of months when stored as a powder compound **1** seems to undergo a phase change as evidenced by a different powder diffractogram and Mössbauer spectrum.

Bis(μ$_{6,7}$-hydrogenphosphato)-tetrakis(μ$_7$-phosphato)diiron(III)-pentairon(II), $^3{}_\infty[Fe^{II}{}_5Fe^{III}{}_2(PO_4)_2(H_{0.5}PO_4)_4]$, (2). Under a positive pressure of argon $FeCl_2\cdot 3H_2O$ (0.353 g, 1.5 mmol) was dispersed in 5 mL of degassed water in a Schlenk flask to give a yellowish–green, clear solution. To this solution *N*-methylpiperazinedium hydrogenphosphate (0.645 g, 3.0 mmol) was added with continuous stirring. The pH of the resulting solution was 3.1. The mixture was stirred at room temperature for 30 min. The solution was transferred to a Teflon-lined stainless-steel autoclave and heated at 180 °C for 40 h followed by slow cooling at a rate of 10 °C min^{-1}. Black–green crystals were collected by filtration (yield 210 mg, quantitative). $Fe_7H_2O_{24}P_6$ (962.78): calc.: C 0.00, H 0.21, N 0.00; found: C 0.00, H 0.00, N 0.00% (note that the hydrogen content of 0.20% falls within the error margin of the CHN instrument). IR (major peaks only): 1457 (νP=O), 1002 (νP–O).

Acknowledgements

The research was supported by the Fonds der Chemischen Industrie and the graduate college "Unpaired electrons" at the University of Freiburg through a fellowship to K. A.-S. We thank Prof. A. X. Trautwein for his support and helpful discussions.

References

1 C. N. R. Rao, S. Natarajan, A. Choudhury, S. Neeraj and A. A. Ayi, *Acc. Chem. Res.*, 2001, **34**, 80.
2 Review: A. K. Cheetham, G. Férey and T. Loiseau, *Angew. Chem., Int. Ed.*, 1999, **38**, 3268.
3 Gallophosphate polymorphs, theory: S. Girard, J. D. Gale, C. Mellot-Draznieks and G. Férey, *J. Am. Chem. Soc.*, 2002, **124**, 1040.
4 $^3{}_\infty\{[C_4N_2H_{12}][Co_{0.14}Zn_{1.86}(PO_4)(H_{1.5}PO_4)_2]\}$: X. Chen, Y. Zhao, R. Wang, M. Li and Z. Mai, *J. Chem. Soc., Dalton Trans.*, 2002, 3092.
5 $^3{}_\infty\{[C_2NH_8][Zn_3(PO_4)(HPO_4)_2]\cdot H_2O\}$ and $^3{}_\infty\{[(C_2NH_8)(H_3O)][Zn_4(PO_4)_3(H_2O)]_2\cdot H_2O\}$: S. Neeraj and A. K. Cheetham, *Chem. Commun.*, 2002, 1738.
6 Open-framework zinc phosphates: Y. Song, J. Yu, G. Li, Y. Li, Y. Wang and R. Xu, *Chem. Commun.*, 2002, 1720.
7 $^2{}_\infty\{[NH_4][(V_2O_3(4,4'\text{-bipy})_2(H_2PO_4)(PO_4)_2]\cdot 0.5H_2O\}$: L.-I. Hung, S.-L. Wang, H.-M. Kao and K.-H. Lii, *Inorg. Chem.*, 2002, **41**, 3929.

8 $^{1}_{\infty}\{[C_6N_2H_{14}][Fe_2F_2(HPO_4)_2(H_2PO_4)_2]\cdot 2H_2O\}$ and $^{3}_{\infty}\{[C_6N_2H_{14}][Fe_3(OH)F_3(PO_4)(H_2PO_4)_2]_2\cdot H_2O\}$: S. Mahesh, M. A. Green and S. Natarajan, *J. Solid State Chem.*, 2002, **165**, 334.

9 $^{2}_{\infty}\{[4,4'\text{-}H_2bipy][V_2(HPO_4)_4(4,4'\text{-}bipy)_2]\}$ (bipy = bipyridine): C.-H. Huang, L.-H. Huang and K.-H. Lii, *Inorg. Chem.*, 2001, **40**, 2625.

10 $^{3}_{\infty}\{[Ga_2(deta)(PO_4)_2]\cdot 2H_2O\}$ (deta = diethylenetriamine): C.-H. Lin, S.-L. Wang and K.-H. Lii, *J. Am. Chem. Soc.*, 2001, **123**, 4649.

11 $^{3}_{\infty}\{[H_3O][AlP_2O_6(OH)_2]\}$: W. Yan, J. Yu, Z. Shi and R. Xu, *Chem. Commun.*, 2000, 1431.

12 Metal phosphates from amine phosphates: C. N. R. Rao, S. Natarajan and S. Neeraj, *J. Solid State Chem.*, 2000, **152**, 302.

13 $^{3}_{\infty}\{[H_3N(CH_2)_4NH_3]_2[Ga_4(HPO_4)(PO_4)_3(OH)_3]\cdot\sim 5.4H_2O\}$: A. M. Chippindale, K. J. Peacock and A. J. Cowley, *J. Solid State Chem.*, 1999, **145**, 379.

14 $^{2}_{\infty}\{[Cu(bipy)_2(VO)_3(PO_4)_2(HPO_4)_2]\cdot 2H_2O\}$ and $^{1}_{\infty}[Cu(terpy)_2(VO_2)_3(PO_4)(HPO_4)_2]$: R. Finn and J. Zubieta, *Chem. Commun.*, 2000, 1321.

15 J. M. Thomas and R. Raja, *Aust. J. Chem.*, 2001, **54**, 551.

16 S. K. Mohapatra, B. Sahoo, W. Keune and P. Selvam, *Chem. Commun.*, 2002, 1466.

17 K. Abu-Shandi, H. Winkler, B. Wu and C. Janiak, *CrystEngComm*, 2003, **5**, 180.

18 E. Roland and P. Kleinschmit, *Ullmann's Encyclopedia of Industrial Chemistry*, VCH, Weinheim, 5th edn., 1996, Vol. A28, p. 475; G. H. Kühl and C. T. Kresge, *Kirk-Othmer Encyclopedia of Chemical Technology*, Wiley, New York, 4th edn., 1995, vol. 16, p. 888; F. Schüth, *Chem. Unserer Zeit*, 1995, **29**, 42; W. Hölderich, M. Hesse and F. Näumann, *Angew. Chem., Int. Ed.*, 1988, **27**, 226; L. Puppe, *Chem. Unserer Zeit*, 1986, **20**, 117.

19 $^{1}_{\infty}[Cu(H_2PO_4)_2(4,4'\text{-}bipy)(H_2O)_2]$: K. Abu-Shandi, C. Janiak and B. Kersting, *Acta Crystallogr., Sect. C*, 2001, **57**, 1261.

20 Reduced molybdenum phosphates: R. C. Haushalter and L. A. Mundi, *Chem. Mater.*, 1992, **4**, 31.

21 $^{1}_{\infty}\{[(HN(CH_2CH_2)_3NH)K_{1.35}][V_5O_9(PO_4)_2]\cdot xH_2O\}$: M. I. Khan, L. M. Meyer, R. C. Haushalter, A. L. Schweiter, J. Zubieta and J. L. Dye, *Chem. Mater.*, 1996, **8**, 43.

22 Review: S. Oliver, A. Kuperman and G. A. Ozin, *Angew. Chem., Int. Ed.*, 1998, **37**, 46.

23 $^{1}_{\infty}\{[Ga_4(C_{10}H_9N_2)_2(PO_4)(H_{0.5}PO_4)_2(HPO_4)_2(H_2PO_4)_2(H_2O)_2]\cdot H_2O\}$: C.-Y. Chen, F. R. Lo, H. M. Kao and K. H. Lii, *Chem. Commun.*, 2000, 1061.

24 $^{1}_{\infty}\{[C_4N_2H_{12}]_2[Cu_2I_6]\cdot H_2O\}$: A. B. Corradi, M. R. Cramarossa, T. Manfredini, L. P. Battaglia, G. Pelosi, A. Saccani and F. Sandrolini, *J. Chem Soc., Dalton Trans.*, 1993, 3587.

25 $^{2}_{\infty}\{[C_4N_2H_{12}]_3[Mo_8O_{27}]\}$: W. T. A. Harrison, L. L. Dussack and A. J. Jacobson, *Acta Crystallogr., Sect. C*, 1996, **52**, 1075.

26 $^{3}_{\infty}\{[C_4N_2H_{12}][(Co_{0.44}Zn_{0.56})_2(PO_4)(H_{1.5}PO_4)_2\}$ and $^{3}_{\infty}\{[C_5N_2H_{14}][(Co_{0.25}Zn_{0.75})(HPO_4)_2]\}$: A. N. Christensen, A. Bareges, R. B. Nielsen, R. G. Hazell, P. Norby and J. C. Hanson, *J. Chem. Soc., Dalton Trans.*, 2001, 1611.

27 $^{1}_{\infty}\{[C_5N_2H_{13}][CoCl_3(C_5N_2H_{12})]\}$: A. Marzotto, D. A. Clemente and G. Valle, *Acta Crystallogr., Sect. C*, 1999, **55**, 43.

28 $^{3}_{\infty}[Fe^{II}_7(PO_4)_2(HPO_4)_4]$: B-C. Zhou, Y-W. Yao and R.-J. Wang, *Acta Crystallogr., Sect. C*, 2002, **58**, i109.

29 E. Craven, K. Abu-Shandi and C. Janiak, *Z. Anorg. Allg. Chem.*, 2003, **629**, 195.

30 Review: P. Gütlich, A. Hauser and H. Spiering, *Angew. Chem., Int. Ed. Engl.*, 1994, **33**, 2024; O. Kahn, *Molecular Magnetism*, VCH, Weinheim, 1993, ch. 4, p. 53ff; J. Zarembowitch, *New. J. Chem.*, 1992, **16**, 255; P. Gütlich and A. Hauser, *Coord. Chem. Rev.*, 1990, **97**, 1; H. Toftlund, *Coord. Chem. Rev.*, 1989, **94**, 67; E. König, *Prog. Inorg. Chem.*, 1987, **35**, 527; P. Gütlich, *Struct. Bonding (Berlin)*, 1981, **44**, 83; H. A. Goodwin, *Coord. Chem. Rev.*, 1976, **18**, 293.

31 B. Kersting, M. J. Kolm and C. Janiak, *Z. Anorg. Allg. Chem.*, 1998, **624**, 775; B. Kersting, D. Siebert, D. Volkmer, M. J. Kolm and C. Janiak, *Inorg. Chem.*, 1999, **38**, 3871; A. Geiß, M. J. Kolm, C. Janiak and H. Vahrenkamp, *Inorg. Chem.*, 2000, **39**, 4037.

32 T. Manago, S. Hayami, H. Oshio, S. Osaki, H. Hasuyama, R. H. Herber and Y. Maeda, *J. Chem. Soc., Dalton Trans.*, 1999, 1001.

33 J. R. D. DeBord, W. M. Reiff, C. J. Warren, R. C. Haushalter and J. Zubieta, *Chem. Mater.*, 1997, **9**, 1994.

34 D. Lee, J. L. DuBois, B. Pierce, B. Hedman, K. O. Hodgson, M. P. Hendrich and S. J. Lippard, *Inorg. Chem.*, 2002, **41**, 3172; W. E. Buschmann, J. Ensling, P. Gütlich and J. S. Miller, *Chem. Eur. J.*, 1999, **5**, 3019; J. R. Haradorn, L. Que, Jr. and W. B. Tolman, *J. Am. Chem. Soc.*, 1999, **121**, 9760; M. Sato, Y. Hayashi, T. Tsuda and M. Katada, *Inorg. Chim. Acta*, 1997, **261**, 113; C.-C. Wu, H. G. Jang, A. L. Rheingold, P. Gütlich and D. N. Hendrickson, *Inorg. Chem.*, 1996, **35**, 4137.

35 N. N. Greenwood and T. C. Gibb, *Mössbauer Spectroscopy*, Chapman and Hall, London, 1971.

36 W. Reiff, J. Manriquez, M. Ward and J. Miller, *Mol. Cryst. Liq. Cryst.*, 1989, **176**, 423.

37 D. Perry, L. Wilson, K. Kunze, L. Maleki, P. Deplano and E. Trogu, *J. Chem. Soc., Dalton Trans.*, 1981, 1294.

38 S. Yamauchi, Y. Sakai and T. Tominaga, *Bull. Chem. Soc. Jpn.*, 1985, **58**, 442.

39 V. Coropceanu, J. L. Brédas, H. Winkler and A. X. Trautwein, *J. Chem. Phys.*, 2002, **116**, 8152.

40 R. M. Smith, A. E. Martell and R. J. Motekaitis, Critically Selected Stability Constants of Metal Complexes, NIST Standard Reference Database 46, Version 5.0, NIST Standard Reference Data, Gaithersburg, USA, 1998.

41 $^{3}_{\infty}\{[C_4N_2H_{12}]_2[(Fe_x(PO_4)_x(HPO_4)_2(H_2O)_2]\cdot H_2O\}$: V. Zima and K. H. Lii, *J. Solid State Chem.*, 1998, **139**, 326.

42 $^{1}_{\infty}\{[C_4N_2H_{12}]_{1.5}[Fe_2(OH)(PO_4)(HPO_4)_2(H_2PO_4)]\cdot 0.5H_2O\}$: V. Zima and K.-H. Lii, *J. Chem.Soc., Dalton Trans.*, 1998, 4109.

43 V. Zima, K.-H. Lii, N. Nguyen and A, Ducouret, *Chem. Mater.*, 1998, **10**, 1914.

44 $^{1}_{\infty}\{[C_5N_2H_{12}][Co(HPO_4)_2]\}$: A. Choudhury, S. Natarajan and C. N. R. Rao, *J. Chem. Soc., Dalton Trans.*, 2000, 2595.

45 $^{1}_{\infty}\{[H_3N(CH_2)_2NH_3][Al(PO_4)(HPO_4)]\}$: I. D. Williams, J. Yu, Q. Gao, J Chen and R. Xu, *Chem. Commun.*, 1997, 1273.

46 $^{1}_{\infty}\{[H_3N(CH_2)_4NH_3][Ga(PO_4)(HPO_4]\}$: A. M. Chippindale, A. D. Bond, A. D. Law and A. R. Cowley, *J. Solid State Chem.*, 1998, **136**, 227.

47 Bond valences (s) calculated from the bond lengths (R) according to $s = \exp(R_0 - R)/B$ and $R_0 = 1.759$ for Fe^{3+}–O or 1.734 for Fe^{2+}–O, $B = 0.37$; Program VALENCE (Version 2.00, February 1993); I. D. Brown, *J. Appl. Crystallogr.*, 1996, **29**, 479.

48 I. D. Brown and R. D. Shannon, *Acta Crystallogr., Sect A*, 1973, **29**, 266; I. D. Brown and K. K. Wu, *Acta Crystallogr., Sect. B*, 1976, **32**, 1957; I. D. Brown and D. Altermatt, *Acta Crystallogr., Sect. B*, 1985, **41**, 244.

49 M. Riou-Cavellec, C. Serre, J. Robino, M. Noguès, J.-M. Grenèche and G. Férey, *J. Solid State Chem.*, 1999, **147**, 122.

50 L.-M. Zheng, H.-H. Song, C.-H. Lin, S.-L. Wang, Z. Hu, Z. Yu and X.-Q. Xin, *Inorg. Chem.*, 1999, **38**, 4618.

51 J. R. D. DeBord, W. M. Reiff, R. C. Haushalter and J. Zubieta, *J. Solid State Chem.*, 1996, **125**, 186.

52 C.-Y. Huang, S.-L. Wang and K.-H. Lii, *J. Porous Mater.*, 1998, **5**, 147.

53 A. Choudhury, S. Natarajan and C. N. R. Rao, *Chem. Commun.*, 1999, 1305.

54 $[Fe_7(PO_4)_5(HPO_4)]$: I. Vencato, L. Moreira, E. Maltievich and Y. Primerano, *J. Braz. Chem. Soc.*, 1994, **5**, 43.

55 $[Fe_7(PO_4)_6]$: Y. Gorbunor, *Sov. Phys. Crystallogr. (Engl. Transl.)*, 1980, **25**, 785.

56 STOE WinXpow, Version 1.06, copyright 1999, STOE & Cie GMBH. ICSD Inorganic Crystal Structure Database, FIZ Karlsruhe, February 1995.

57 τ = (difference between the two largest anges)/60 for five-coordinated metal centers allows for the assignment of square-pyramidal (ideally $\tau = 0$) or trigonal-biypramidal (ideally $\tau = 1$): A. W. Addison, T. N. Rao, J. Reedijk, J. van Rijn and G. C. Verschoor, *J. Chem. Soc., Dalton Trans.*, 1984, 1349.

58 H. Lueken, Magnetochemie, Teubner Verlag, Stuttgart, 1999, p. 418.

59 SMART, Data Collection Program for the CCD Area-Detector System; SAINT, Data Reduction and Frame Integration Program for the CCD Area-Detector System. Bruker Analytical X-ray Systems, Madison, Wisconsin, USA, 1997.

60 G. Sheldrick, Program SADABS: Area-detector absorption correction, University of Göttingen, Germany, 1996.

61 G. M. Sheldrick, SHELXS-97, SHELXL-97, Programs for Crystal Structure Analysis, University of Göttingen, Germany, 1997.

62 DIAMOND 2.1e for Windows. Crystal Impact Gbr, Bonn, Germany; http://www.crystalimpact.com/diamond.